RSC Applied Polymers

ROYAL SOCIETY OF CHEMISTRY

PAPER

View Article Online
View Journal | View Issue

Check for updates

Cite this: *RSC Appl. Polym.*, 2025, **3**, 1637

Tailorability of moisture barrier and mechanical performance in clay-based multilayer nanocomposite thin films

Rahul Manna,†[a] Sarah G. Fisher,†[b] Margaret J. Karim,[b] Darrell Setiawan,[d] Alexandra V. Moran,[d] Jaime C. Grunlan *[b,c,d] and Kyungjin Kim *[a,e,f]

Clay-based nanocomposites have gained significant interest in the last few years due to their biocompatibility and potential applications in food packaging, wearables, and flame-retardant coatings. Among existing manufacturing methods, layer-by-layer (LbL) deposition of multilayer films with nanoclays has shown the ability to produce extremely well aligned platelets with controllable nanoscale thickness, and has also been shown to improve gas barrier performance. In contrast, the equally important moisture barrier performance and mechanical properties have not been thoroughly explored. This study focuses on the performance of three types of LbL films consisting of polyethyleneimine (PEI), polyacrylic acid (PAA), and montmorillonite (MMT) or vermiculite (VMT) nanoclays, resulting in PEI/VMT bilayer (BL) films, PEI/VMT/PEI/PAA quadlayer (QL) films, and PEI/MMT/PEI/PAA QL films on a polyethylene terephthalate substrate. Surface roughness as low as 26.2 ± 4.9 nm and inorganic platelet content as high as 96.7 ± 1.1 wt% are achieved with the VMT BL films. This highly aligned, densely packed, high aspect ratio platelet structure enables a water vapor transmission rate (WVTR), at 50% relative humidity and 37 °C, as low as 720.9 mg m^{-2} day^{-1} for a 500 nm thin VMT BL. High stiffness values are estimated for all coatings: 162.47 GPa, 70.94 GPa, and 37.06 GPa for 500 nm VMT BL, VMT QL, and MMT QL films, respectively. A high elastic limit is observed in MMT QL cracking with crack onset strains exceeding 5%, attributed to the higher organic content compared to the BL and the smaller aspect ratio of MMT platelets compared to VMT. These trends observed in moisture barrier and mechanical durability performances across BL *vs.* QL and VMT *vs.* MMT highlight the importance of tailored design criteria for optimizing coating applications.

Received 26th August 2025,
Accepted 4th October 2025

DOI: 10.1039/d5lp00265f

rsc.li/rscapplpolym

Open Access Article. Published on 06 October 2025. Downloaded on 2/5/2026 12:16:35 AM.
This article is licensed under a Creative Commons Attribution 3.0 Unported Licence.

1. Introduction

Clay-based nanoflake thin-films are layered nanomaterials derived from natural or synthetic clays, characterized by their high aspect ratio and large surface area.[1,2] Due to their unique structural, mechanical, barrier, and biocompatible properties, they have garnered significant interest for applications in nanocomposites, coatings, and environmental remediation.[2,3] With potential uses in food packaging,[4–7] flexible electronics,[4,8] wearables,[2,9] implantable devices,[2,10,11] and flame-retardant coatings,[12–14] these films can be optimized for a wide range of applications by altering the materials or manufacturing processes.[15] Clay nanoparticles are excellent building blocks for barrier coatings because their high aspect ratio platelets create highly tortuous diffusion pathways that effectively resist the transport of gases and moisture.[16–19] Among thin-film technologies, clay-based barriers provide higher gas and moisture resistance than organic coatings,[20–23] and, while maintaining mechanical flexibility, have the potential to approach the high barrier levels of vacuum-processed conformal inorganic coatings, which are typically brittle and prone to cracking.[24–28]

Layer-by-layer (LbL) deposition is a process of building thin-films by alternating deposition of polymers, nanoparticles (such as clays), and molecules to create films with exceptionally well controlled distribution, and alignment that allows nanoscale ultra-thin LbL thickness.[4,13,29,30] The adhesion between the alternating layers is primarily dependent on the

[a]*Department of Mechanical Engineering, University of Connecticut, Storrs, CT, 06269, USA. E-mail: kyungjin.kim@uconn.edu*
[b]*Department of Chemistry, Texas A&M University, College Station, TX, 77843, USA. E-mail: jgrunlan@tamu.edu*
[c]*Department of Materials Science and Engineering, Texas A&M University, College Station, TX, 77843, USA*
[d]*Department of Mechanical Engineering, Texas A&M University, College Station, TX, 77843, USA*
[e]*Institute of Materials Science, University of Connecticut, Storrs, CT, USA*
[f]*Department of Biomedical Engineering, University of Connecticut, Storrs, CT, USA*
†These two authors contributed equally to this manuscript and are joint first authors.

© 2025 The Author(s). Published by the Royal Society of Chemistry

Open Access Article. Published on 06 October 2025. Downloaded on 2/5/2026 12:16:35 AM.
This article is licensed under a Creative Commons Attribution 3.0 Unported Licence.

electrostatic interactions between oppositely charged aqueous polyelectrolytes and nanoparticles.[3,31,32] This technique offers enhanced versatility in film design and optimization. For instance, film thickness can be tuned by adjusting the number of deposition cycles, while surface properties can be tailored by modifying the ionic strength or adjusting the pH of each solution.[8,32–35] Additionally, parameters such as temperature, exposure time, and molecular weight can be controlled to further refine film characteristics and achieve the desired characteristics and performance.[4,36]

For clay-based nanocomposites, LbL deposition provides better barrier performance compared to films that have been manufactured by randomly dispersing clay platelets in a polymer matrix and deionized water.[3,4,37] Previous studies have developed ultra-thin, highly-transparent LbL films with alternating bilayers (BL) of highly aligned and exfoliated montmorillonite (MMT) or vermiculite (VMT) clay nanoparticles and polyethyleneimine (PEI) that achieved exceptional gas barrier properties, with oxygen transmission rates (OTR) less than 0.005 cm^3 per (m^2 day atm).[4,21] In another study, bilayers comprised of MMT and polyacrylamide (PAM) assembled *via* LbL deposition also yielded thin films with similarly high gas barrier performance.[38] Furthermore, LbL films incorporating a sequence of three materials, *i.e.* MMT, PEI, and polyacrylic acid (PAA), have been explored, where each unit sequence of PEI/MMT/PEI/PAA is referred to as a quadlayer.[18,39–42] These films achieved the same exceptional gas barrier performance with a mere 4 QL or 16 total layers. Different sequences of PEI, nanoclay (NC), and PAA such as PEI/NC/PAA have further been explored and found to be very high gas barriers.[42] Polyelectrolytes such as PEI and PAA provide strong control over layer thickness and film growth through pH adjustment, potentially yielding improved performance. For instance, lowering the pH of PEI in a PEI/MMT system reduced the oxygen transmission rate (OTR) by a factor of 20 while decreasing the elastic modulus by a factor of 2.[21] This improvement results from the increased clay density and concentration at lower pH, which generate longer, more tortuous diffusion pathways and thereby enhance barrier performance without increasing film thickness. Alternating PEI and PAA between layers of clay to create quadlayer films has been shown to yield highly interdiffused polyelectrolyte layers, leading to exponential film growth and superior gas barrier performance in ultra-thin films.[18,43] Similarly, a study developed quadlayer and hexlayer systems with branched PEI (BPEI), MMT, and hydrophobic fluorinated polymer Nafion in a sequence of BPEI/MMT/BPEI/Nafion and ((BPEI/Nafion)$_2$/BPEI/MMT) on PLA substrate which achieved significant reduction in both oxygen and water vapor permeability.[44] Although relatively few studies have explored the mechanical properties of LbL-deposited films with clay platelets, those that have report exceptional performance. For example, films with linear polyethyleneimine (LPEI), MMT, and PAA in a sequence of LPEI/MMT/LPEI/PAA have shown a high elastic modulus of 45 GPa and a tensile strength of 70 MPa with a 20 QL film.[40]

Preceding work in the area on LbL nanoclay composites has primarily been focused on evaluating and improving gas barrier performance. In most applications such as flexible electronics and food packaging, the moisture barrier performance mechanical integrity are equally important to consider.[7,45,46] Incorporation of nanoclays in polymers has previously been shown to improve both mechanical and moisture barrier performance.[19,46–49] While the properties of MMT based LbL and randomly dispersed films have been explored extensively before, LbL films with VMT are yet to be developed and assessed.[14,50,51] Vermiculite, known for its exceptional water holding capacity, self-repairing ability, and proton conductivity, can potentially provide films with high gas and moisture performance with durable properties.[52–54]

In this work, we focus on the tunability of moisture barrier and mechanical properties in clay-based multilayer thin films, as these characteristics are particularly critical for sustainable food packaging and flexible electronic applications. By demonstrating how structural modifications influence these properties, our study provides a framework for optimizing film performance toward specific end uses. To this end, we develop three types of LbL films consisting of PEI/VMT bilayers, PEI/VMT/PEI/PAA quadlayers, and PEI/MMT/PEI/PAA quadlayers on polyethylene terephthalate (PET) substrates. The barrier, mechanical, and fragmentation performance of these films with thickness of 100 nm, 250 nm, and 500 nm are evaluated by determining the water vapor transmission rate with a permeation analyzer and the mechanical properties through *in situ* optical microscopy tensile tests. These films achieve a magnitude lower WVTR than previously tested MMT-based randomly dispersed nanocomposites, with a significantly higher estimated film stiffness. These results highlight the significant improvement in moisture barrier and mechanical performance across the board with the incorporation of VMT in LbL self-assembled films.

2. Materials and methods

Materials and solution preparation

Branched polyethyleneimine (PEI, M_w = 25 000 g mol^{-1}), poly (acrylic acid) (PAA, M_w = 250 000 g mol^{-1}, 35 wt% in water), and sodium hydroxide (NaOH, ACS reagent, pellets) were purchased from MilliporeSigma (Burlington, MA, USA). Hydrochloric acid (HCl, 5.0 N) was purchased from VWR International (Radnor, PA, USA). Vermiculite clay (VMT, microlite 963++, 7.8 wt% in water) was purchased from Specialty Vermiculite Corp (Winnipeg, MB, Canada), and sodium montmorillonite (MMT, Cloisite-Na+) was purchased from BYK (Gonzales, TX, USA). VMT clay platelets have been reported to have a diameter of 1.1 μm while MMT clay platelets are known to have a platelet diameter range of 10–1000 nm.[21,55] Poly (ethylene terephthalate) (PET) film (179 μm thick) was purchased from Tekra (New Berlin, WI, USA) and was used as the substrate for barrier testing. Polished 500 μm-thick undoped silicon wafers were purchased from University Wafer (Boston, MA, USA) and were used as the substrates for thickness measurements, atomic force microscopy, and thermo-

© 2025 The Author(s). Published by the Royal Society of Chemistry

Open Access Article. Published on 06 October 2025. Downloaded on 2/5/2026 12:16:35 AM. This article is licensed under a Creative Commons Attribution 3.0 Unported Licence.

gravimetric analysis. All solutions were prepared using 18 MΩ deionized (DI) water. PEI solutions were prepared at 0.1 wt%, stirred for 24 hours, and adjusted to pH 10 with 1 M HCl. PAA solutions were prepared at 0.2 wt%, stirred for 24 hours, and adjusted to pH 4 with 1 M NaOH. MMT and VMT solutions were prepared at 2 wt% and stirred for 24 hours. VMT solutions were used at their unaltered pH (~7), while MMT solutions were adjusted to pH 6 using 1 M HCl. The chemical structures of PEI, PAA, MMT, and VMT are depicted in Fig. 1a.

Film fabrication

PET substrates were corona-treated and silicon wafers were plasma-treated immediately before coating to improve film adhesion. The coating procedure for each system is summarized in Fig. 1b. For the VMT bilayer system, the treated substrate was immersed in the PEI solution for 5 minutes, then rinsed with DI water and dried with compressed air. The substrate was then immersed in the VMT solution for 5 minutes, rinsed with DI water, and dried with compressed air to complete the first BL. Subsequent bilayers proceeded as described for the first BL, but the dip time was shortened to 1 minute. For the quadlayer systems, the treated substrate was immersed in the PEI solution for 5 minutes, then rinsed with DI water and dried with compressed air. The substrate was then immersed in the PAA solution for 5 minutes, rinsed with DI water, and dried with compressed air. Next the substrate was immersed in a second PEI solution for 1 minute, rinsed with DI water, and dried with compressed air. Finally, the substrate was immersed in the clay solution (either VMT or MMT) for 1 minute, rinsed with DI water, and dried with compressed air to complete the first QL. Subsequent quadlayers proceeded as described for the first QL, but the dip time was shortened to 1 minute for all layers.

Thickness and surface characterization

Film thickness was measured in triplicate using a P6 profilometer (KLA–Tencor, Milpitas, CA, USA). Unless otherwise specified, all films were grown to ~500 nm for characterization. A quartz crystal microbalance (QCM, Maxtek Inc., Cypress, CA, USA) was utilized to determine the area density (mass per area) of the films at set layer numbers. A Bruker Dimension Icon atomic force microscope (AFM, Billerica, MA, USA) was used to evaluate the surface morphology and roughness of the LbL films. Samples for thermogravimetric analysis (TGA) were prepared by scraping the LbL coatings off of their silicon wafer substrates with a razor blade. TGA was performed in duplicate for each type of film using a Discovery TGA 55 (TA Instruments, New Castle, DE, USA). ~0.8 mg samples were heated isothermally at 120 °C for 20 minutes to remove any

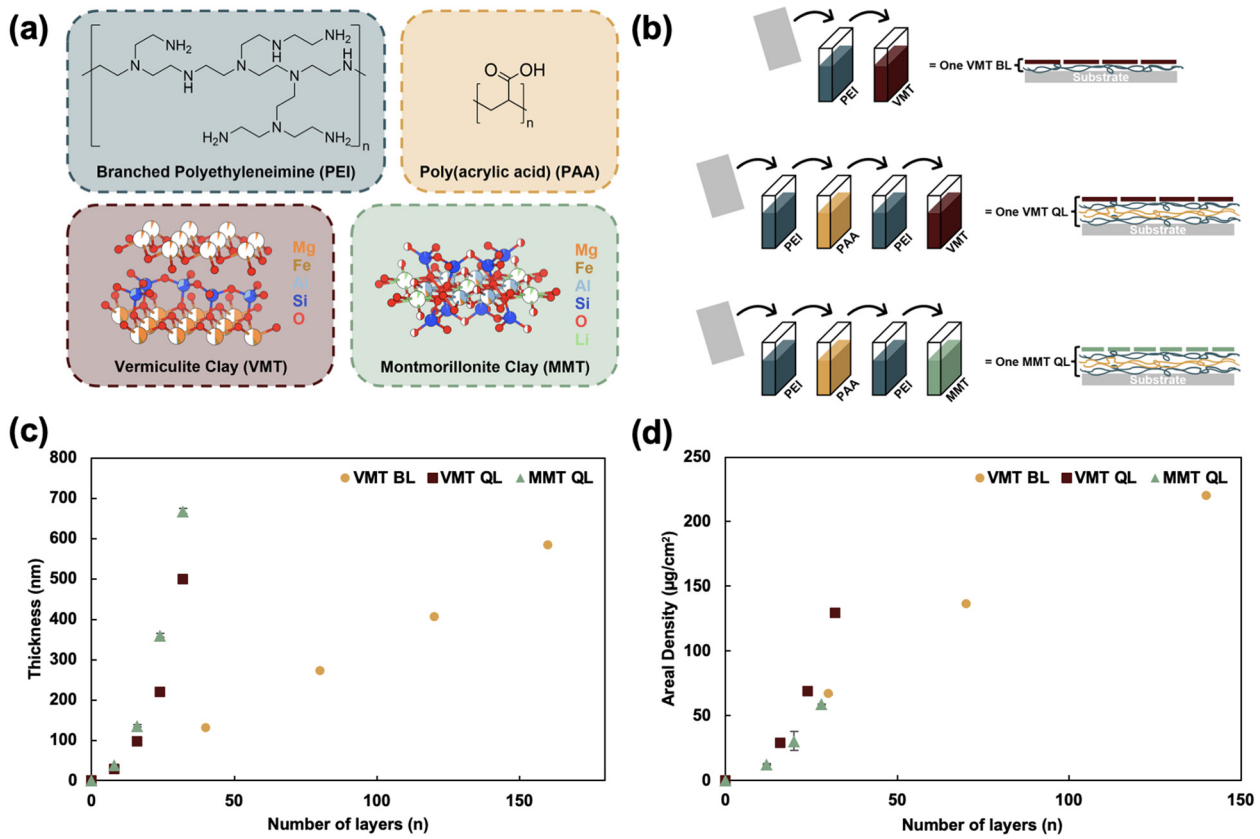

Fig. 1 (a) Chemical structures of film components, (b) schematic of LbL film deposition process, and (c) film thickness and (d) areal density as a function of layer number ($2n$ = 1 BL, $4n$ = 1 QL).

Open Access Article. Published on 06 October 2025. Downloaded on 2/5/2026 12:16:35 AM. This article is licensed under a Creative Commons Attribution 3.0 Unported Licence.

residual water, after which the temperature was increased by 10 °C min^{-1} up to 900 °C under an air flow of 60 mL s^{-1}.

Mechanical testing and damage analysis

All three types of films, each with thickness of 100 nm, 250 nm, and 500 nm, on 179 μm PET substrates, were scissors-cut into 5 mm by 35 mm strips. Tensile tests were conducted on all the samples on a Linkam Modular Force Stage Micro tensile tester with a 200 N load cell and a Linkam T96s controller operated through the OEM LINK software. The tests were conducted at room temperature and humidity (21 °C and 30% RH) *in situ* under a Nikon Eclipse LV100N POL optical microscope with a 2048 × 1536 resolution FLIR Grasshopper 3 camera (GS3-U3-32S4C-C) to record and analyze crack evolution in the films at 15 frames per second. No preconditioning was performed before testing. Around four to five samples were stretched uniaxially under monotonic loading at a displacement rate 60 μm s^{-1}, which lies within the range where PET viscoelasticity is not expected to significantly alter results.[56] This displacement rate was chosen to ensure high-quality imaging in a timely manner with the samples being stretched 1% in approximately 3 seconds. Prior to testing, calipers (Fisherbrand 14-648-17) were used to determine the average width of each sample. The thickness of each specimen was measured with a 1 μm-resolution micrometer (Mitutoyo 293-340-30) to confirm the initial measurements. Since the thickness measurements through profilometry were deemed more reliable and the micrometer measurements showed low variance, a fixed thickness was used along with the measured average width to calculate the cross-sectional area and subsequently the engineering stress for each sample. The elastic modulus of the film-substrate system was determined by performing a simple linear regression on a subset of collected data under 2% strain as this was found to be below the yield point for all tested samples. The coating moduli are estimated by subtracting substrate modulus from total (film-substrate) modulus for each sample, *i.e.* $E_f = (E_tA_t - E_sA_s)/A_f$ where E_t is defined as the total modulus, A_t is the total area, E_s is defined as the substrate modulus, A_s is the total area, and A_f is the film area. Additionally, *in situ* recordings of samples under tensile load were analyzed frame-by-frame in VLC media player to determine crack onset strain (COS) for all tested samples by identifying the first growing crack(s).

Water vapor transmission rate testing

The water vapor transmission rates of all three types of films on PET each with coating thicknesses of 100 nm, 250 nm, and 500 nm were tested in a AMETEK MOCON Aquatran 3 Permeation Analyzer following the ASTM F3299 standard. The Bare PET was not tested as previous studies indicated that its permeation would exceed the analyzer's detection limit of 5 g m^{-2} day^{-1}. Since measurements above this threshold would be unreliable, a standard literature value of 5000 mg m^{-2} day^{-1} at 37 °C and 40% RH was assumed instead.[57] Foil masks (AMETEK 052-612) with a 5 cm^2 area were used to prepare the samples for testing at 37 °C. Airgas Ultra High Purity 99.999% Nitrogen (NI UHP300) was used as the carrier gas. All the samples were tested at 50% relative humidity (RH), while the 500 nm samples were additionally tested at 100% RH. The permeation analyzer strictly maintains the relative humidity at the specified value. Prior to measurement, each sample was conditioned in the analyzer at the defined humidity and temperature for 48 hours to ensure measurement stability and accuracy. The tests were stopped once the measurements were observed to be saturated with less than 5% change between subsequent measurements. WVTR values of the coating were extracted, and a substrate WVTR of 5500 mg m^{-2} day^{-1} was assumed to provide a conservative estimate of the coating performance.

3. Results and discussion

Film growth

Fig. 1c shows film thickness as a function of layer number n ($2n$ = 1 BL, $4n$ = 1 QL) and the data is provided in Table S1. It is immediately apparent that the BL film grows significantly thinner per layer than the QL films, with 20 BL (40 total layers) being required to achieve ~100 nm of thickness (*versus* 4 QL or 16 total layers). Fig. S1 compares linear and exponential fits of film thickness *versus* layer number, with high R^2 for the linear fit in VMT BL films and the exponential fit in QL films. This is attributed to the mechanism of layer deposition. The QL films' exponential growth is attributed to the "in-and-out" interdiffusion of the weak polyelectrolytes PEI and PAA during deposition.[39,58] This mechanism of growth is commonly observed in polyelectrolyte multilayer films,[59,60] and is not dramatically affected by the incorporation of clay nanoplatelet layers as long as there are still interfaces between oppositely charged polyelectrolytes in the film.[58] In contrast, the BL film contains only cationic PEI and anionic VMT, so there are no interfaces for interpolymer diffusion during film deposition. This leads to a substantially thinner, linear growth regime compared to the quadlayer films, as has been observed previously.[21,55,58] In the bilayer films, a linear growth regime is established within 40 layers (and likely far earlier). In contrast, at 32 total layers, the QL films are still exhibiting exponential thickness growth, which is expected to become linear eventually as a limit of chain interpenetration is reached.[58,61,62] The MMT QL films grow slightly thicker than VMT QL. This is likely because VMT platelets have an aspect ratio ~10× that of MMT.[55,63] Therefore, it is expected that VMT will be somewhat more effective at blocking polyelectrolyte diffusion between clay layers than MMT, leading to thinner growth at the same number of layers. Films were grown to ~500 nm (70 BL for the VMT BL system, 8 QL for the VMT QL system, or 7 QL for the MMT QL system) for characterization unless otherwise specified.

QCM experiments, summarized in Fig. 1d, measure areal density of each LbL system as a function of layer number, with the data provided in Table S2. In agreement with the film thickness trend, the QL systems show exponential increases

© 2025 The Author(s). Published by the Royal Society of Chemistry

Open Access Article. Published on 06 October 2025. Downloaded on 2/5/2026 12:16:35 AM.
This article is licensed under a Creative Commons Attribution 3.0 Unported Licence.

Table 1 Number of layers, extrapolated density, inorganic content, and roughness of LbL films

System	Number of layers at ~500 nm	Extrapolated density (g cm^{-3})	Inorganic content (wt%)	Average roughness (nm)	Root mean square roughness (nm)
VMT BL	70 BL	2.56	96.7 ± 1.1	26.2 ± 4.9	36.4 ± 8.1
VMT QL	8 QL	1.79	37.8 ± 0.9	72.0 ± 23.0	95.7 ± 28.9
MMT QL	7 QL	1.82	58.6 ± 10.6	43.4 ± 11.1	55.6 ± 12.2

(Fig. S2) in mass due to exponential polyelectrolyte deposition with increasing layer numbers. In contrast, the VMT BL film exhibits a nearly linear mass increase with respect to layer number. The film density is extrapolated from QCM data by dividing the areal mass by the measured film thickness at the maximum number of layers (Table 1). The VMT and MMT QL systems have very similar extrapolated densities of 1.79 and 1.82 g cm^{-3}, while the VMT BL film has a much higher density of 2.56 g cm^{-3}. This is likely due to the BL system having a substantially higher volume fraction of inorganic clay, as observed in previous studies.[39,55] Lower density in the QL systems is due to interpolymer diffusion causing the spacing between clay layers in the polymer matrix to be much greater, leading to lower clay volume fraction overall. The significantly higher clay content of the BL system is confirmed *via* thermogravimetric analysis. Fig. S3 shows the degradation of each coating under air. As all polymer content is expected to degrade well below 900 °C,[64,65] the mass remaining at the end of the test is attributed exclusively to clay content. These inorganic content values, listed in Table 1, confirm that the VMT BL system indeed has a much higher weight fraction of clay (>90%) as compared to the QL coatings (~40–60%).

Surface morphology

Atomic force microscopy reveals the surface topology and roughness of the films. Fig. 2 shows AFM height images and phase mapping images of each LbL film. The films appear fairly uniform, with the cobblestone-like structure indicating that the platelets are closely packed and well-oriented.[39,66] As shown in Table 1, all of the films are relatively smooth (average roughness <100 nm), but the roughness varies significantly depending on the clay type and whether the film is a BL or QL system. The VMT BL film has by far the lowest average roughness (26 nm), while the VMT QL film is about 3× rougher. This is likely explained by the difference in the growth mechanisms between the two films. While the BL film grows in thin, uniform layers that maintain the flat and smooth profile of the underlying substrate, the QL film grows in a noticeably thicker deposition per cycle. The thicker polymer layers between each clay layer may result in less even platelet deposition, resulting in greater roughness. It has been observed that in a bilayer system of PEI and MMT, LbL films with thicker organic layers exhibit rougher surfaces in AFM.[21] This also explains why the average roughness of the MMT QL film is less than the VMT

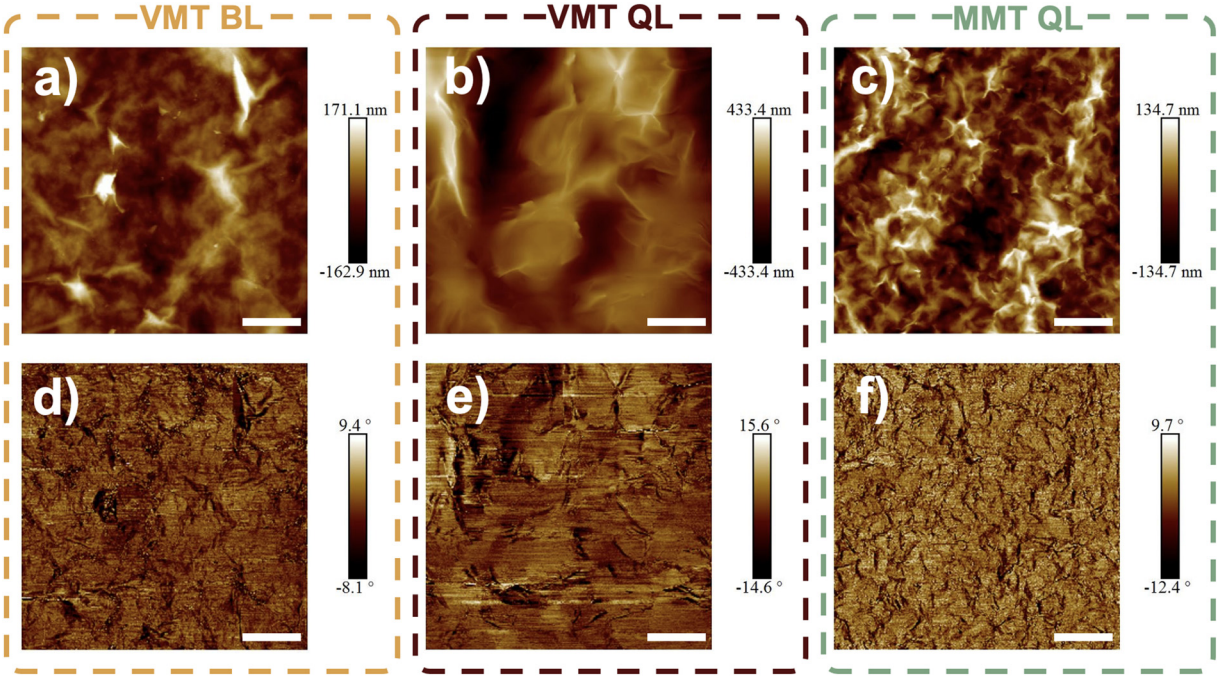

Fig. 2 (a–c) Height and (d–f) phase images of coating on Si wafers. Scale bars are 2 μm.

Open Access Article. Published on 06 October 2025. Downloaded on 2/5/2026 12:16:35 AM.
This article is licensed under a Creative Commons Attribution 3.0 Unported Licence.

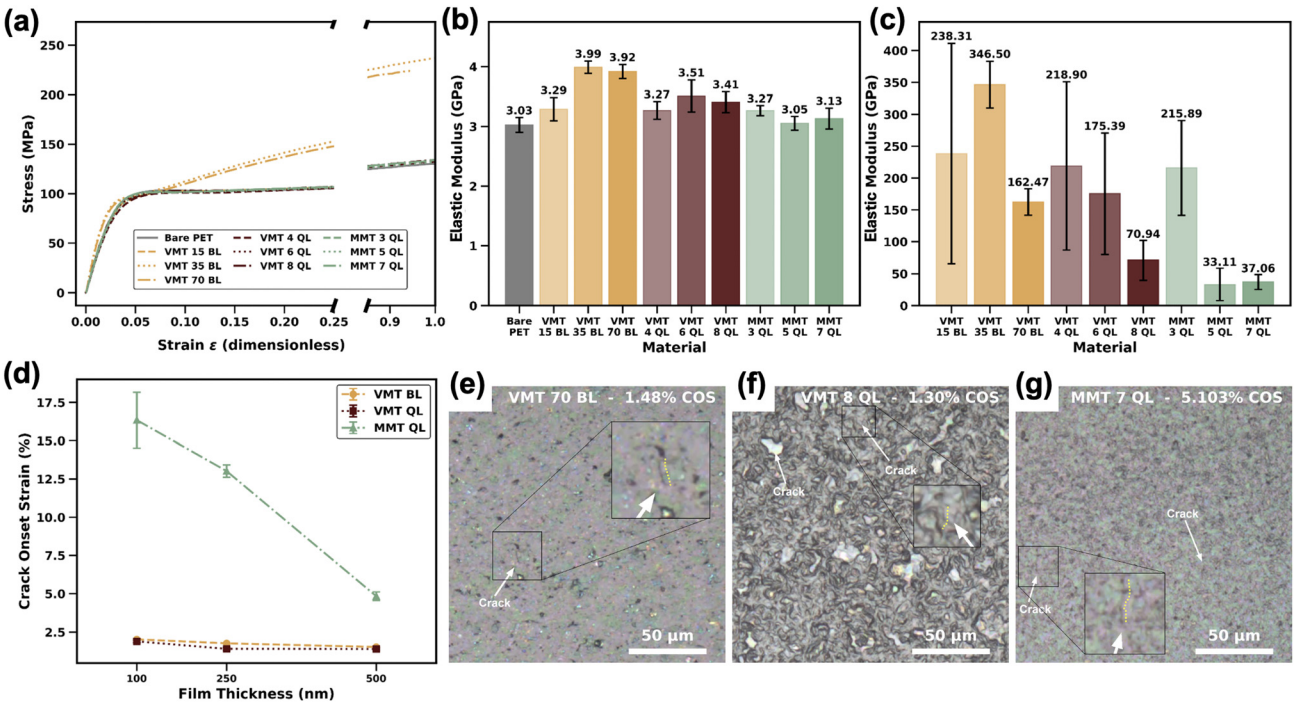

Fig. 3 (a) Engineering stress strain curves of all tested films on PET substrate, (b) film-substrate elastic moduli, and (c) extracted coating moduli. (d) Crack onset strains (COSs) and (e–g) optical images of 500 nm VMT 70 BL, VMT 8 QL and MMT 7 QL films at COS.

QL, but greater than the VMT BL. The thicker polyelectrolyte layers between the platelets in the quadlayer lead to less even deposition than in the BL system, but the unevenly deposited MMT platelets do not increase the roughness as much as the VMT platelets do because they have a much lower aspect ratio. Roughness measurements made on smaller films areas (5 × 5 and 2 × 2 μm scans) generally agree with the trend reported above (Table S3).

Mechanical properties

The results of the mechanical testing are summarized in Fig. 3. The engineering stress strain curve for all the tested films on PET is presented in Fig. 3a. Notably, the VMT 35 BL (250 nm) and the 70 BL (500 nm) film-substrate systems exhibit higher stiffness and strength (260.02 and 223.45 MPa, respectively), than the rest of the samples (~145 MPa). It is likely that the improved strength in the thinner VMT 15 BL films (100 nm), compared to the 35 and 70 BL films, may have been obscured by the relatively thick PET substrate layer. Meanwhile, the mechanical behavior of remaining samples is largely similar to the uncoated PET substrate. The elastic modulus shown in Fig. 3b for all coated samples are determined to be higher than the modulus for uncoated PET, with the VMT 35 BL and 70 BL samples having the highest values of 3.99 and 3.92 GPa, respectively. The estimated coating modulus is higher in VMT BL films than the VMT QL and MMT QL films. This is likely due to the higher content of brittle inorganic platelets in bilayer films, as well as the thicker polymer layers in quadlayer films, which contribute to reduced coating stiffness. The VMT QL films show the second-highest coating modulus and the MMT QL films show the lowest among the samples tested. This difference is attributed to the lower aspect ratio of MMT platelets compared to VMT (~10× lower), which results in a higher pre-crack density in MMT QL films and thus allows greater elastic deformation. Average film moduli of 162.47 GPa for the VMT 70 BL films, 70.94 GPa for the VMT 8 QL films, and 37.06 GPa for the MMT 7 QL films were determined. Additionally, an increase in film thickness corresponds to a notable decrease in the estimated film modulus. This trend is especially prominent in QL films due to the exponential increase in thickness with layer number, as more polymer content accumulates. In contrast, bilayer films exhibit a linear increase in thickness with the number of layers (15, 35, 70) and the decreasing trend in modulus is not as apparent. However, it is possible that the modulus decreases more noticeably beyond 120 layers, as the film thickness increases beyond a linear progression (Fig. 1c). Finally, it should be noted that these results may carry some uncertainty, as they depend on the accuracy of the measured cross-sectional areas and the estimated film–substrate modulus, rather than direct testing of the film alone. Since the film thickness is much smaller than that of the substrate, even minor variations in coating thickness can lead to error propagation in the modulus estimates. This is reflected in the relatively high standard deviation of the estimated coating moduli for the thinner 100 nm films (Fig. 3c) and the reduced deviation observed as film thickness increases across all systems. However, profilometry measurements (Table S1) confirmed

© 2025 The Author(s). Published by the Royal Society of Chemistry

Open Access Article. Published on 06 October 2025. Downloaded on 2/5/2026 12:16:35 AM. This article is licensed under a Creative Commons Attribution 3.0 Unported Licence.

that the films were highly uniform, with very low variation, supporting the overall reliability of the results.

In situ microscope images reveal the MMT films exhibit significantly higher crack onset strain (COS) values than the VMT films with the MMT 7 QL film, showing an average COS of approximately 4.84%. In the case of the MMT 3 QL and 5 QL films (100 nm and 250 nm thick, respectively), the high COS involves substantial local plastic deformation of the PET substrate, and thus the values may be somewhat inaccurate, but they still indicate a high elastic limit of the coatings above 5%. The low aspect ratio of MMT platelets compared to VMT platelets, and the resulting higher density of pre-cracks in MMT films, likely leads to less fracture energy being required to initiate flake (Mode I) cracking. Regardless of whether the LbL structure is QL or BL, the flake layers in the stack undergo in-plane stress distribution under uniaxial tensile loading. Therefore, the COS values of the VMT BL and QL films remain fairly similar, in the range of 1–2%. The crack onset strain images are shown in Fig. 3e and f. A decrease in COS with increasing thickness is observed across all film types. Since the MMT QL films exhibit high COS, this reduction is more pronounced than in the VMT BL and QL films. The inverse relationship between COS and film thickness aligns with the expectations of linear elastic fracture mechanics for homogeneous inorganic coatings, following COS $\sim 1/(\text{thickness})^{1/2}$.[26,56,67–69] The fact that our LbL composite films follow this trend suggests that the flake layers are uniformly distributed throughout the observed area, indicating a high degree of coating homogeneity. The *in situ* microscopy tensile testing images of crack propagation, presented in Fig. 4, highlight distinct fragmentation behaviors across film types. In the VMT BL films, cracks propagate more rapidly, with visible crack joining and bridging. In contrast, cracks in the VMT QL films grow more independently and at a slower rate, likely due to the lower inorganic content, approximately 2.5× less than in the VMT BL films, along the thickness direction. The greater polymer content in VMT QL films at equivalent thickness allows cracks to propagate more slowly, delaying their merging and the formation of new cracks. On the other hand, crack bridging occurs earlier in the VMT BL films, due to the thinner polymer layers separating the densely packed VMT flakes. Meanwhile, the MMT QL films exhibit significantly smaller cracks and slower crack propagation, which can be attributed to the smaller aspect ratio of MMT platelets and the higher polymer content compared to VMT BL films.

Water vapor barrier properties

The WVTR testing results are shown in Fig. 5 and the time-dependent saturation of WVTR is shown in Fig. S6. Among the samples tested, VMT QL and VMT BL films exhibit similar and the lowest WVTR values at 50% RH. The VMT 8 QL shows a WVTR of 819.4 mg m^{-2} day^{-1}, while the VMT 70 BL shows a

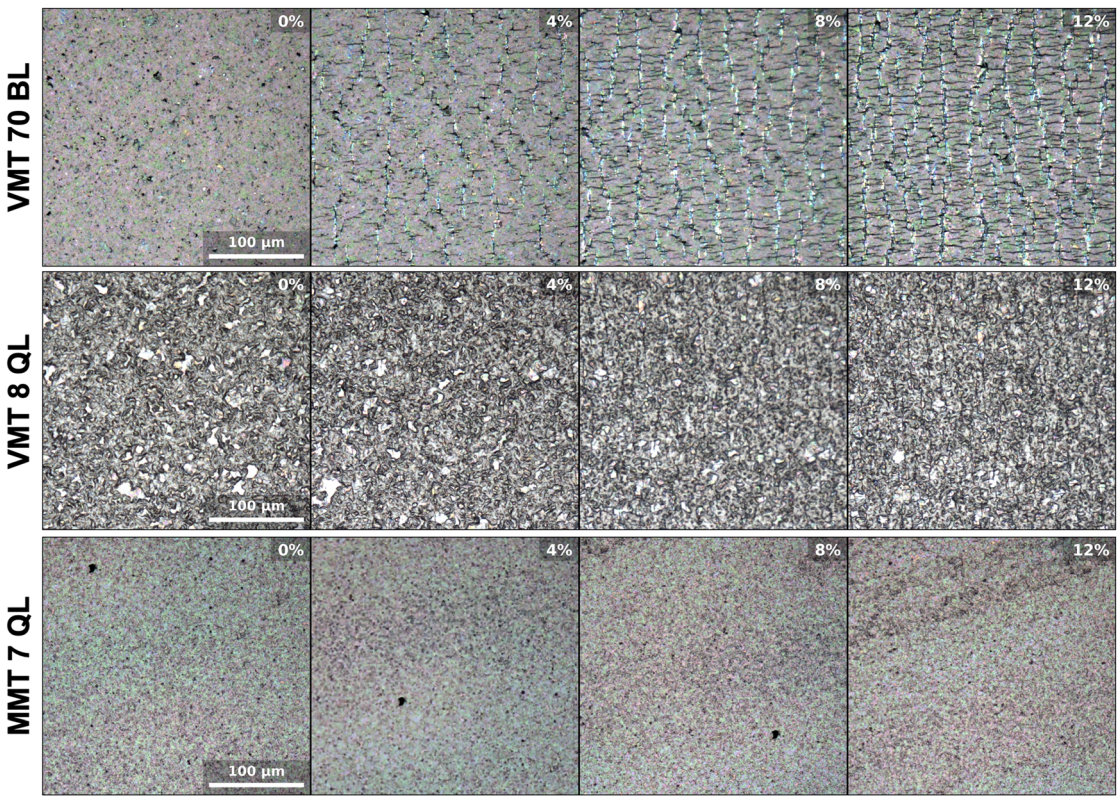

Fig. 4 *In situ* mechanical testing images of ~500 nm films on PET, from 0% to 12% strain (left to right) in 2% increments. Images after saturation of 500 nm films and control images of PET are provided in Fig. S4 and S5, respectively.

Open Access Article. Published on 06 October 2025. Downloaded on 2/5/2026 12:16:35 AM.
This article is licensed under a Creative Commons Attribution 3.0 Unported Licence.

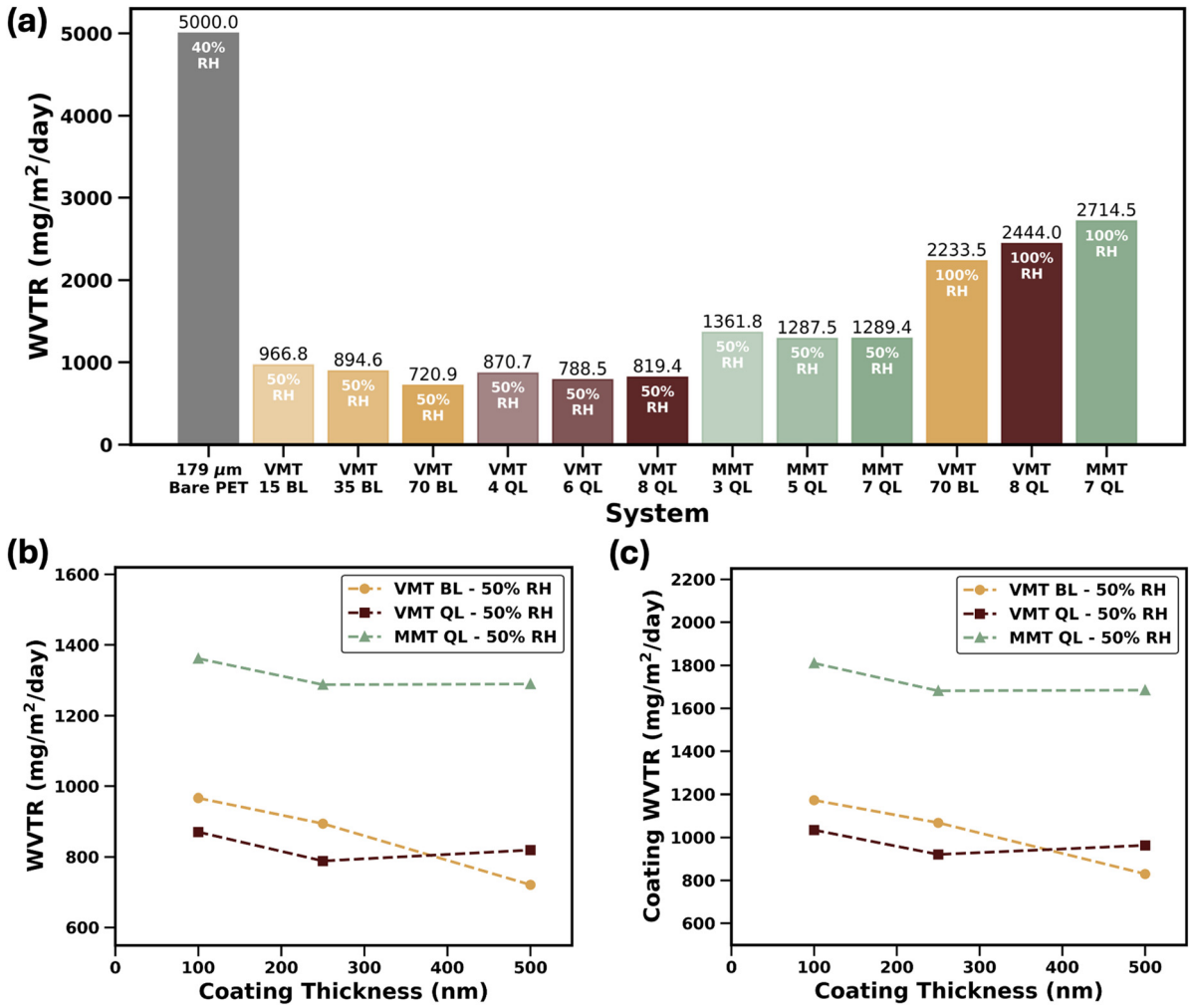

Fig. 5 (a) Water vapor transmission rate of 178 μm PET at 40% RH.[57] WVTR of all tested films at 50% RH, except WVTR of VMT 70 BL, VMT 8 QL, and MMT 7 QL at 100% RH. All films were tested at 37 °C. (b) WVTR vs coating thickness for films tested at 50% RH. (c) Extracted WVTR of the coating for films tested at 50% RH with $WVTR_{Substrate} \approx 5500$ mg m^{-2} day^{-1}.

lower value of 720.9 mg m^{-2} day^{-1}. In contrast, MMT QL films display significantly higher WVTR values at all tested thicknesses, with the MMT 7 QL film reaching 1289.4 mg m^{-2} day^{-1}. A similar trend is observed at 100% RH, with WVTR values of 2233.5 mg m^{-2} day^{-1} for the VMT 70 BL, 2444 mg m^{-2} day^{-1} for the VMT 8 QL, and 2714.5 mg m^{-2} day^{-1} for the MMT 7 QL. For reference, uncoated 178 μm PET has a reported WVTR of ~5000 mg m^{-2} day^{-1} at 40% RH and 37 °C.[50,57] Surface roughness does not appear to be a primary driver of barrier performance; rather, clay platelet identity and number of organic layers play a more significant role. Previous publications report a WVTR of 1418 mg m^{-2} day^{-1} at 100% RH and 23 °C for a VMT 30 BL film (226 nm thick) on a biaxially oriented polypropylene substrate.[70] Another study reports 650 mg m^{-2} day^{-1} for a VMT 20 BL film (165 nm thick) on a PET substrate at 100% RH and 23 °C, along with an OTR of 0.071 cm^3 m^{-2} day^{-1} atm under the same conditions (Table 2).[55] These differences between previously reported WVTR values and the current results likely stem from the exponential relationship between WVTR and temperature.[57,71] According to the manufacturer of the permeation analyzer, WVTR can increase by 6% to 15% for every degree Celsius increase in temperature for many barriers. Thus, for the 14 °C difference in this case, the WVTR at 37 °C can be expected to be 2–7 times higher than the value measured at 23 °C. Increasing the number of layers and overall film thickness leads to only a modest reduction in total WVTR (Fig. 5b) and coating WVTR (Fig. 5c) for the MMT QL and VMT QL films (Fig. 5b), while a steady decrease is observed in VMT BL films as the number of bilayers increases. This trend likely results from the denser BL structure and higher aspect ratio of VMT platelets, which create more tortuous diffusion pathways compared to the QL structure and MMT platelets, respectively. These findings support the strategy of increasing the number of bilayers in VMT BL films to achieve lower WVTR values and improved barrier performance. Based on previously reported results (Table 2), all the LbL coatings investigated in this work are also expected to exhibit excellent (undetectable or near-undetectable) oxygen transmission rate values.

© 2025 The Author(s). Published by the Royal Society of Chemistry

Table 2 Barrier properties of VMT and MMT based LbL films tested and previously reported

System	Thickness (nm)	Dry OTR [0% RH, 23 °C] (cm^3 per m^2 per day atm)	Humid OTR [100% RH, 23 °C] (cm^3 per m^2 per day atm)	WVTR [100% RH, 23 °C] (mg per m^2 per day atm)	WVTR [50% RH, 37 °C] (mg per m^2 per day atm)	WVTR [100% RH, 37 °C] (mg per m^2 per day atm)
VMT 70 BL, this work	500	—	—	—	720.9	2233.5
VMT 8 QL, this work	500	—	—	—	819	2444
MMT 7 QL, this work	500	—	—	—	1289.4	2714.5
VMT 20 BL[55]	165	0.017	0.071	650	—	—
MMT 3 QL[39,62]	44	<0.005	—	—	—	—
MMT 7 QL[32]	Not reported	<0.005	0.1395	—	—	—

All barrier values were obtained using 179 μm PET as the substrate.

While the barrier improvement factor observed for the films tested is moderate, the high tunability of the VMT BL films offers considerable potential. By tailoring increasing thickness, these films can potentially achieve enhanced barrier performance and higher improvement factors, underscoring their promise for specialized applications. These films are best suited for uses where tunable barrier and mechanical performance are valued over large-scale throughput, offering a cost-effective solution for areas such as flexible electronics and food packaging. However, the simplicity of the fabrication method highlights its potential for adaptation to advanced processing techniques, which could enable industrial-scale implementation.

4. Conclusion

PEI/VMT BL films, PEI/VMT/PEI/PAA QL films, and PEI/MMT/PEI/PAA QL films were studied in regard to their barrier and mechanical performance. As the number of layers increases, film thickness in the VMT and MMT QL systems grows exponentially due to interdiffusion between the polyelectrolytes PEI and PAA, while the VMT BL films exhibit linear thickness growth, attributed to the absence of interfaces for interpolymer diffusion. The films are characterized using AFM and TGA, and their performance is evaluated through *in situ* microscopy tensile testing and WVTR measurements. In addition to the VMT's high aspect ratio, VMT BL films demonstrate superior mechanical and barrier performance compared to QL films, owing to their higher inorganic content (96.7 ± 1.1 wt%) and lower surface roughness (26.2 ± 4.9 nm). Therefore, higher resistance to structural deformation and tortuous diffusion pathways result in higher stiffness (162.47 GPa), higher strength (260.02 MPa), and a lower WVTR (720.9 mg m^{-2} day^{-1}) for a 500 nm coating. Higher elastic limits are therefore observed in MMT QL films, with crack onset strains exceeding 5%, attributed to their higher organic content and the smaller aspect ratio of MMT platelets compared to VMT. These trends in moisture barrier and mechanical durability performance across BL *vs.* QL and VMT *vs.* MMT underscore the importance of tailored design strategies for optimizing advanced coating applications.

Conflicts of interest

The authors declare no conflict of interest.

Data availability

The data supporting this article are included in the supplementary information (SI). Supplementary information: materials characterization for each coating assembly, including TGA analysis to assess thermal stability and water vapor transmission rate studies to evaluate moisture barrier performance. See DOI: https://doi.org/10.1039/d5lp00265f.

Acknowledgements

This work was supported under Cooperative Agreement W56HZV-21-2-0001 with the US Army DEVCOM Ground Vehicle Systems Center (GVSC), through the Virtual Prototyping of Autonomy Enabled Ground Systems (VIPR-GS) program. Distribution statement A. Approved for public release; distribution is unlimited. OPSEC9942. This material is also based upon work supported by the National Science Foundation Graduate Research Fellowship Program under Grant No. DGE-2139772. Any opinions, findings, and conclusions or recommendations expressed in this material are those of the author(s) and do not necessarily reflect the views of the National Science Foundation.

References

1 E. A. Franco-Urquiza, Clay-Based Polymer Nanocomposites: Essential Work of Fracture, *Polymers*, 2021, **13**, 2399.
2 P. Das, *et al.*, Current synthesis and characterization techniques for clay-based polymer nano-composites and its biomedical applications: A review, *Environ. Res.*, 2022, **212**, 113534.
3 I. Soltani, S. D. Smith and R. J. Spontak, Effect of polyelectrolyte on the barrier efficacy of layer-by-layer nanoclay coatings, *J. Membr. Sci.*, 2017, **526**, 172–180.

Open Access Article. Published on 06 October 2025. Downloaded on 2/5/2026 12:16:35 AM. This article is licensed under a Creative Commons Attribution 3.0 Unported Licence.

Open Access Article. Published on 06 October 2025. Downloaded on 2/5/2026 12:16:35 AM. This article is licensed under a Creative Commons Attribution 3.0 Unported Licence.

4 C. Cho, F. Xiang, K. L. Wallace and J. C. Grunlan, Combined Ionic and Hydrogen Bonding in Polymer Multilayer Thin Film for High Gas Barrier and Stretchiness, *Macromolecules*, 2015, **48**, 5723–5729.
5 S. Jali, T. P. Mohan, F. M. Mwangi and K. Kanny, A Review on Barrier Properties of Cellulose/Clay Nanocomposite Polymers for Packaging Applications, *Polymers*, 2023, **16**, 51.
6 K. Y. Perera, A. K. Jaiswal and S. Jaiswal, Biopolymer-Based Sustainable Food Packaging Materials: Challenges, Solutions, and Applications, *Foods*, 2023, **12**, 2422.
7 J. R. Rocca-Smith, *et al.*, Toward Sustainable PLA-Based Multilayer Complexes with Improved Barrier Properties, *ACS Sustainable Chem. Eng.*, 2019, **7**, 3759–3771.
8 G. Rydzek, *et al.*, Electrochemical nanoarchitectonics and layer-by-layer assembly: From basics to future, *Nano Today*, 2015, **10**, 138–167.
9 E. Barrett-Catton, M. L. Ross and P. Asuri, Multifunctional Hydrogel Nanocomposites for Biomedical Applications, *Polymers*, 2021, **13**, 856.
10 T. F. Mohammed Fitri, *et al.*, Biomedical PEVA Nanocomposite with Dual Clay Nanofiller: Cytotoxicity, Mechanical Properties, and Biostability, *Polymers*, 2021, **13**, 4345.
11 U. Raza and K. Kim, Reliability Analysis of Soft Pib-Hbn Nanocomposite Barriers for Diffusion and Thermal Management in Flexible Implantable Applications, SSRN Scholarly Paper, 2025. DOI:DOI: 10.2139/ssrn.5344485.
12 Y.-C. Li, *et al.*, Flame Retardant Behavior of Polyelectrolyte–Clay Thin Film Assemblies on Cotton Fabric, *ACS Nano*, 2010, **4**, 3325–3337.
13 A. Fahami, J. Lee, S. Lazar and J. C. Grunlan, Mica-Based Multilayer Nanocoating as a Highly Effective Flame Retardant and Smoke Suppressant, *ACS Appl. Mater. Interfaces*, 2020, **12**, 19938–19943.
14 F. Ding, *et al.*, Biomimetic nanocoatings with exceptional mechanical, barrier, and flame-retardant properties from large-scale one-step coassembly, *Sci. Adv.*, 2017, **3**, e1701212.
15 Q. H. Zeng, A. B. Yu, G. Q. Lu and D. R. Paul, Clay-Based Polymer Nanocomposites: Research and Commercial Development, *J. Nanosci. Nanotechnol.*, 2005, **5**, 1574–1592.
16 S. Qin, Y. Song, M. E. Floto and J. C. Grunlan, Combined High Stretchability and Gas Barrier in Hydrogen-Bonded Multilayer Nanobrick Wall Thin Films, *ACS Appl. Mater. Interfaces*, 2017, **9**, 7903–7907.
17 D. R. Paul and L. M. Robeson, Polymer nanotechnology: Nanocomposites, *Polymer*, 2008, **49**, 3187–3204.
18 P. Tzeng, E. L. Lugo, G. D. Mai, B. A. Wilhite and J. C. Grunlan, Super Hydrogen and Helium Barrier with Polyelectolyte Nanobrick Wall Thin Film, *Macromol. Rapid Commun.*, 2015, **36**, 96–101.
19 C. M. O. Müller, J. B. Laurindo and F. Yamashita, Effect of nanoclay incorporation method on mechanical and water vapor barrier properties of starch-based films, *Ind. Crops Prod.*, 2011, **33**, 605–610.
20 J. Wang, *et al.*, Moisture and Oxygen Barrier Properties of Cellulose Nanomaterial-Based Films, *ACS Sustainable Chem. Eng.*, 2018, **6**, 49–70.
21 M. A. Priolo, D. Gamboa and J. C. Grunlan, Transparent Clay–Polymer Nano Brick Wall Assemblies with Tailorable Oxygen Barrier, *ACS Appl. Mater. Interfaces*, 2010, **2**, 312–320.
22 M. Mariello, K. Kim, K. Wu, S. P. Lacour and Y. Leterrier, Recent advances in encapsulation of flexible bioelectronic implants: materials, technologies and characterization methods, *Adv. Mater.*, 2022, 2201129, DOI: 10.1002/adma.202201129.
23 M. Niemiec and K. Kim, Lifetime engineering of bioelectronic implants with mechanically reliable thin film encapsulations, *Prog. Biomed. Eng.*, 2023, **6**, 012001.
24 K. Kim, *et al.*, Extended Barrier Lifetime of Partially Cracked Organic/Inorganic Multilayers for Compliant Implantable Electronics, *Small*, 2021, **17**, 2103039.
25 M. Niemiec, F. Bayansal, N. Biyikli and K. Kim, Failure behavior of polymer microelectrode arrays encapsulated with conventional ALD and 3D-ALI barriers, *Front. Bioeng. Biotechnol.*, 2025, **13**, 1622927.
26 K. Kim, S. Graham and O. N. Pierron, Note: A single specimen channel crack growth technique applied to brittle thin films on polymer substrates, *Rev. Sci. Instrum.*, 2017, **88**, 036102.
27 K. Kim, *Mechanical reliability of thin barrier films for flexible electronics*, Georgia Institute of Technology, 2018.
28 C. Diyaroglu, M. T. M. Anaei and K. Kim, A finite element framework on water vapor transmission rates by pinhole damages in inorganic ultrabarriers for flexible electronics, *Appl. Surf. Sci.*, 2024, **659**, 159870.
29 G. Decher, Layer-by-Layer Assembly (Putting Molecules to Work), in *Multilayer Thin Films*, ed. G. Decher and J. B. Schlenoff, Wiley, 2012, pp. 1–21. DOI: 10.1002/9783527646746.ch1.
30 S. J. Percival, *et al.*, Nanoscale thin film corrosion barriers enabled by multilayer polymer clay nanocomposites, *Surf. Coat. Technol.*, 2020, **383**, 125228.
31 M. A. Priolo, K. M. Holder, T. Guin and J. C. Grunlan, Recent Advances in Gas Barrier Thin Films via Layer-by-Layer Assembly of Polymers and Platelets, *Macromol. Rapid Commun.*, 2015, **36**, 866–879.
32 E.-H. Song, *et al.*, Highly Oriented Gold/Nanoclay–Polymer Nanocomposites for Flexible Gas Barrier Films, *ACS Appl. Mater. Interfaces*, 2015, **7**, 4778–4783.
33 D. T. Haynie, S. Balkundi, N. Palath, K. Chakravarthula and K. Dave, Polypeptide Multilayer Films: Role of Molecular Structure and Charge, *Langmuir*, 2004, **20**, 4540–4547.
34 P. Bieker and M. Schönhoff, Linear and Exponential Growth Regimes of Multilayers of Weak Polyelectrolytes in Dependence on pH, *Macromolecules*, 2010, **43**, 5052–5059.
35 Y. Yang, L. Bolling, M. A. Priolo and J. C. Grunlan, Super Gas Barrier and Selectivity of Graphene Oxide–Polymer Multilayer Thin Films, *Adv. Mater.*, 2013, **25**, 503–508.
36 D. A. Hagen, B. Foster, B. Stevens and J. C. Grunlan, Shift-Time Polyelectrolyte Multilayer Assembly: Fast Film Growth

© 2025 The Author(s). Published by the Royal Society of Chemistry

Open Access Article. Published on 06 October 2025. Downloaded on 2/5/2026 12:16:35 AM. This article is licensed under a Creative Commons Attribution 3.0 Unported Licence.

and High Gas Barrier with Fewer Layers by Adjusting Deposition Time, *ACS Macro Lett.*, 2014, **3**, 663–666.
37 F.-X. Xiao, J. Miao and B. Liu, Layer-by-Layer Self-Assembly of CdS Quantum Dots/Graphene Nanosheets Hybrid Films for Photoelectrochemical and Photocatalytic Applications, *J. Am. Chem. Soc.*, 2014, **136**, 1559–1569.
38 W.-S. Jang, I. Rawson and J. C. Grunlan, Layer-by-layer assembly of thin film oxygen barrier, *Thin Solid Films*, 2008, **516**, 4819–4825.
39 M. A. Priolo, D. Gamboa, K. M. Holder and J. C. Grunlan, Super Gas Barrier of Transparent Polymer–Clay Multilayer Ultrathin Films, *Nano Lett.*, 2010, **10**, 4970–4974.
40 C. Cho, *et al.*, Nanobrick wall multilayer thin films grown faster and stronger using electrophoretic deposition, *Nanotechnology*, 2015, **26**, 185703.
41 D. A. Hagen, *et al.*, High gas barrier imparted by similarly charged multilayers in nanobrick wall thin films, *RSC Adv.*, 2014, **4**, 18354–18359.
42 T. Gulin-Sarfraz, *et al.*, Optimized multilayer coating using layer-by-layer assembly method for excellent oxygen barrier of poly(lactic acid) based film, *Colloids Surf., A*, 2023, **664**, 131155.
43 D. A. Hagen, *et al.*, Balancing polyelectrolyte diffusion and clay deposition for high gas barrier, *Green Mater.*, 2016, **4**, 98–103.
44 F. Carosio, *et al.*, Efficient Gas and Water Vapor Barrier Properties of Thin Poly(lactic acid) Packaging Films: Functionalization with Moisture Resistant Nafion and Clay Multilayers, *Chem. Mater.*, 2014, **26**, 5459–5466.
45 B. Tan and N. L. Thomas, A review of the water barrier properties of polymer/clay and polymer/graphene nanocomposites, *J. Membr. Sci.*, 2016, **514**, 595–612.
46 M. N. Uddin, *et al.*, Research and applications of nanoclays: A review, *SPE Polym.*, 2024, **5**, 507–535.
47 V. Ojijo, S. Sinha Ray and R. Sadiku, Effect of Nanoclay Loading on the Thermal and Mechanical Properties of Biodegradable Polylactide/Poly[(butylene succinate)-co-adipate] Blend Composites, *ACS Appl. Mater. Interfaces*, 2012, **4**, 2395–2405.
48 M. Shettar, C. S. S. Kowshik, M. Manjunath and P. Hiremath, Experimental investigation on mechanical and wear properties of nanoclay–epoxy composites, *J. Mater. Res. Technol.*, 2020, **9**, 9108–9116.
49 T. P. Mohan and K. Kanny, Water barrier properties of nanoclay filled sisal fibre reinforced epoxy composites, *Composites, Part A*, 2011, **42**, 385–393.
50 C. Diyaroglu, *et al.*, Full range fragmentation simulation of nanoflake filler-matrix composite coatings on a polymer substrate, *Extreme Mech. Lett.*, 2024, **73**, 102268.
51 M.-J. Dumont, A. Reyna-Valencia, J.-P. Emond and M. Bousmina, Barrier properties of polypropylene/organoclay nanocomposites, *J. Appl. Polym. Sci.*, 2007, **103**, 618–625.
52 K. Raidongia and J. Huang, Nanofluidic Ion Transport through Reconstructed Layered Materials, *J. Am. Chem. Soc.*, 2012, **134**, 16528–16531.
53 J. Deka, K. Saha, A. Yadav and K. Raidongia, Clay-Based Nanofluidic Membrane Derived from Vermiculite Nanoflakes for Pressure-Responsive Power Generation, *ACS Appl. Nano Mater.*, 2021, **4**, 4872–4880.
54 W. Wang, and A. Wang, Vermiculite Nanomaterials: Structure, Properties, and Potential Applications, in *Nanomaterials from Clay Minerals*, Elsevier, 2019, pp. 415–484. DOI: 10.1016/B978-0-12-814533-3.00009-0.
55 M. A. Priolo, K. M. Holder, S. M. Greenlee and J. C. Grunlan, Transparency, Gas Barrier, and, Moisture Resistance of Large-Aspect-Ratio Vermiculite Nanobrick Wall Thin Films, *ACS Appl. Mater. Interfaces*, 2012, **4**, 5529–5533.
56 K. Kim, *et al.*, Environmentally Assisted Cracking in Silicon Nitride Barrier Films on Poly(ethylene terephthalate) Substrates, *ACS Appl. Mater. Interfaces*, 2016, **8**, 27169–27178.
57 N. G. Dhere, Flexible packaging for PV modules, *Proc. SPIE 7048, Reliability of Photovoltaic Cells, Modules, Components, and Systems*, 2008, 70480R, DOI: 10.1117/12.795718.
58 P. Podsiadlo, *et al.*, Exponential Growth of LBL Films with Incorporated Inorganic Sheets, *Nano Lett.*, 2008, **8**, 1762–1770.
59 C. Wang, *et al.*, Recent advances of nanocomposite membranes using layer-by-layer assembly, *J. Membr. Sci.*, 2022, **661**, 120926.
60 J. B. Schlenoff and S. T. Dubas, Mechanism of Polyelectrolyte Multilayer Growth: Charge Overcompensation and Distribution, *Macromolecules*, 2001, **34**, 592–598.
61 C. Porcel, *et al.*, Influence of the Polyelectrolyte Molecular Weight on Exponentially Growing Multilayer Films in the Linear Regime, *Langmuir*, 2007, **23**, 1898–1904.
62 D. A. Hagen, *et al.*, Balancing polyelectrolyte diffusion and clay deposition for high gas barrier, *Green Mater.*, 2016, **4**, 98–103.
63 D. A. Hagen, L. Saucier and J. C. Grunlan, Controlling Effective Aspect Ratio and Packing of Clay with pH for Improved Gas Barrier in Nanobrick Wall Thin Films, *ACS Appl. Mater. Interfaces*, 2014, **6**, 22914–22919.
64 I. Coralli, *et al.*, Analytical pyrolysis of polyethyleneimines, *J. Anal. Appl. Pyrolysis*, 2023, **169**, 105838.
65 I. C. McNeill and S. M. T. Sadeghi, Thermal stability and degradation mechanisms of poly(acrylic acid) and its salts: Part 1—Poly(acrylic acid), *Polym. Degrad. Stab.*, 1990, **29**, 233–246.
66 P. Tzeng, C. R. Maupin and J. C. Grunlan, Influence of polymer interdiffusion and clay concentration on gas barrier of polyelectrolyte/clay nanobrick wall quadlayer assemblies, *J. Membr. Sci.*, 2014, **452**, 46–53.
67 K. Kim, *et al.*, Optimizing Crack Onset Strain for Silicon Nitride/Fluoropolymer Nanolaminate Barrier Films, *ACS Appl. Nano Mater.*, 2019, **2**, 2525–2532.
68 K. Kim, O. N. Pierron and S. Graham, Atomic layer deposited Al_2O_3 capping layer effect on environmentally assisted cracking in SiNx barrier films, *J. Appl. Phys.*, 2019, **125**, 045301.

© 2025 The Author(s). Published by the Royal Society of Chemistry

69 K. Kim, H. Luo, T. Zhu, O. N. Pierron and S. Graham, Influence of Polymer Substrate Damage on the Time Dependent Cracking of SiNx Barrier Films, *Sci. Rep.*, 2018, **8**, 4560.
70 Y. Song, P. Tzeng and J. C. Grunlan, Super Oxygen and Improved Water Vapor Barrier of Polypropylene Film with Polyelectrolyte Multilayer Nanocoatings, *Macromol. Rapid Commun.*, 2016, **37**, 963–968.
71 S. Kiese, E. Kücükpinar, O. Miesbauer and H.-C. Langowski, The influence of temperature on the intrinsic transport properties of water in inorganic and polymeric coatings, *Thin Solid Films*, 2021, **717**, 138476.

Open Access Article. Published on 06 October 2025. Downloaded on 2/5/2026 12:16:35 AM.
This article is licensed under a Creative Commons Attribution 3.0 Unported Licence.

© 2025 The Author(s). Published by the Royal Society of Chemistry